Realizing vector meson dominance with transverse charge densities

G. A. Miller, M. Strikman, and C. Weiss

Realizing vector meson dominance with transverse charge densities

G. A. Miller,[1] M. Strikman,[2] and C. Weiss[3]

[1]*Department of Physics, University of Washington, Seattle, WA 98195–1560, USA*
[2]*Department of Physics, Pennsylvania State University, University Park, PA 16802, USA*
[3]*Theory Center, Jefferson Lab, Newport News, VA 23606, USA*
(Dated: May 25, 2010)

The transverse charge density in a fast–moving nucleon is represented as a dispersion integral of the imaginary part of the Dirac form factor in the timelike region (spectral function). At a given transverse distance b the integration effectively extends over energies in a range $\sqrt{t} \lesssim 1/b$, with exponential suppression of larger values. The transverse charge density at peripheral distances thus acts as a low–pass filter for the spectral function and allows one to select energy regions dominated by specific t–channel states, corresponding to definite exchange mechanisms in the spacelike form factor. We show that distances $b \sim 0.5 - 1.5$ fm in the isovector density are maximally sensitive to the ρ meson region, with only a $\sim 10\%$ contribution from higher–mass states. Soft–pion exchange governed by chiral dynamics becomes relevant only at larger distances. In the isoscalar density higher–mass states beyond the ω are comparatively more important. The dispersion approach suggests that the positive transverse charge density in the neutron at $b \sim 1$ fm, found previously in a Fourier analysis of spacelike form factor data, could serve as a sensitive test of the the isoscalar strength in the ~ 1 GeV mass region. In terms of partonic structure, the transverse densities in the vector meson region $b \sim 1$ fm support an approximate mean–field picture of the motion of valence quarks in the nucleon.

I. INTRODUCTION

Elastic electron scattering is one of the principal sources of information on the nucleon's spatial size and its internal structure. Two different physical pictures have traditionally been invoked to interpret the nucleon form factors measured in such experiments. The first imagines the nucleon as an extended object in space, characterized by a distribution of charge and current, and aims to explain the form factors as the Fourier image of these spatial distributions. This approach has been used extensively in non-relativistic nuclear physics, where electron scattering has provided detailed spatial images of the charge and current distribution in nuclei. The other picture views elastic scattering as the exchange of a meson–like system between the current and the nucleon and attempts to describe the form factors in terms of the masses and couplings of these hadronic states. Historically, the existence of vector mesons was first postulated in order to explain the observed behavior of the nucleon form factors in the region of spacelike momentum transfers $|t| \lesssim 1$ GeV^2 [1]. The equivalence of the "extended object" and "exchange mechanism" viewpoints is rooted in fundamental properties of strong interactions, namely their relativistic invariance and causality. They guarantee the existence of dispersion relations that express the form factors at spacelike momentum transfers in terms of their imaginary parts in the timelike domain (or spectral functions), where the exchange mechanisms correspond to intermediate hadronic states in the hypothetical process of nucleon–antinucleon creation by the electromagnetic current.

It is generally expected that a more quantitative comparison between the two pictures might provide useful insights into nucleon structure. Generally, one hopes that in this way one may relate the physical density of charge and current at a given distance to exchange mechanisms of a certain mass. However, such studies were long rendered unattractive by the fact that the conventional spatial representation of form factors, in terms of three–dimensional spatial distributions in the Breit frame (zero energy transfer), is meaningful only for non-relativistic systems. These distributions have no proper density interpretation in the relativistic case [2, 3] and cannot be related to observables in processes other than elastic eN scattering. The Breit frame distributions produced by the well-known exchange mechanisms were studied in several works, but it has proved difficult to interpret the results outside of this particular context [4–6].

A new approach to this problem is possible with the concept of transverse densities [7], whose properties were explored in a series of recent articles [2, 3, 8, 9]. They are defined as 2–dimensional Fourier transforms of the elastic form factors and describe the distribution of charge and magnetization in the plane transverse to the direction of motion of a fast–moving system. In contrast to the Breit frame distributions, they are proper densities and permit a spatial interpretation also for systems in which the motion of the constituents is essentially relativistic, such as hadrons in QCD. In fact, the transverse densities are closely related to the parton picture of hadron structure in high–energy processes and correspond to a reduction of the generalized parton distributions (or GPDs) describing the distribution of quarks/antiquarks with respect to

longitudinal momentum and transverse position [10, 11]. As such, they have an objective meaning beyond low–energy elastic eN scattering and can be related to observables in certain high–energy deep–inelastic processes sensitive to the transverse sizes of the nucleon, such as exclusive and diffractive eN and NN scattering [12]. This places the study of transverse densities in the wider context of exploring the nucleon's partonic structure and allows one to employ concepts of partonic dynamics to interpret the resulting spatial distributions.

In this article we study the transverse charge densities in the nucleon's periphery in a dispersion representation which reveals the connection between partonic structure and the exchange mechanisms acting in the nucleon form factors. This approach was used previously to obtain the chiral large–distance component of the charge density from a theoretical calculation of the isovector spectral function near threshold [8]. Here we perform a more extensive analysis using empirical spectral functions determined in an dispersion fit to nucleon form factor data [13], which include the vector meson region and the high–mass continuum and cover both the isovector and isoscalar channels. Our study reveals several interesting aspects of the transverse charge densities.

First, the transverse distance b provides an external parameter which allows one to effectively select different energy (or mass) regions in the spectral function. This happens thanks to the exponential convergence of the dispersion integral for the transverse density, which strongly suppresses the contribution of energies $\sqrt{t} > 1/b$. In particular, we show that distances $b \sim 0.5 - 1.5$ fm maximally emphasize the ρ meson mass region in the isovector spectral function, with only a $\sim 10\%$ contribution from higher–mass states. In the isoscalar channel the contribution from higher–mass states above the ω are comparatively larger, but the ω can be isolated by going to larger distances of ~ 2 fm. The transverse densities at these distances represent, to our knowledge, the cleanest "vector dominance" observables, permitting detailed study of the vector meson couplings to the nucleon in spacelike (exchange) kinematics.

Second, the dispersion result for the transverse charge densities confirms a slightly positive density in the neutron at intermediate distances $b \sim 0.5 - 1.5$ fm, found previously in a Fourier analysis of the spacelike nucleon form factors [2]. While not unexpected — the spectral functions were constructed to fit the spacelike form factor data — this allows us to discuss this result from a t–channel perspective. The dispersion approach clearly shows that the "pion cloud" becomes relevant only at distances $b \gtrsim 2$ fm, and that the positive density at intermediate distances is dual to vector meson exchange, with important contributions from higher–mass isoscalar states. Their dynamical interpretation remains a challenging problem and is related to the question of the strangeness content of the nucleon. Measurements of the neutron charge density thus may be able to constrain the couplings of these states to the nucleon.

Third, the dispersion results provide new insight into the nucleon's partonic structure. By constructing the ratio of u and d valence quark transverse densities in the nucleon we show that the "vector dominance" region $b \sim 1$ fm is consistent with an approximate mean–field picture of the motion of valence quarks in the nucleon, as suggested by quark models. Our approach allows us to formulate this duality in a model–independent manner, preparing the ground for dynamical model studies.

The plan of this paper is as follows. In Sec. II we discuss the basic properties of the dispersion representation of transverse densities, focusing on the role of the distance b as a filter for energies $\sqrt{t} \sim 1/b$ in the spectral function. In Sec. III we summarize present knowledge of the isovector spectral function and study the contributions of the different energy regions to the transverse density, using the empirical parametrization of Ref. [13]. We identify the region of ρ meson dominance and quantify the corrections resulting from higher–mass states. Appendix A explains in detail how this analysis relates to our earlier study of the chiral component of the isovector transverse density using chiral perturbation theory [8]. In Sec. IV we consider the isoscalar charge density and study its sensitivity to the ω meson pole in the spectral function. We also estimate its uncertainty at large b and discuss at what momentum transfers future measurements of the (spacelike) isoscalar form factor would have the strongest impact on the determination the ωNN coupling. In Sec. V we use our results to study the proton and neutron transverse charge density in the spectral representation. In Sec. VI we extract the transverse densities of u and d quarks in the dispersion approach and discuss the implications for the nucleon's partonic structure. A summary and outlook are presented in Sec. VII.

The dispersion representation can in principle be applied to study transverse densities at any distance, provided one has sufficient information on the relevant spectral functions. In this work we focus on the peripheral region of $b \gtrsim 0.5$ fm, where the densities are dominated by the low–mass singularities that are well constrained by theoretical arguments and fits to present form factor data. While we use the parametrization of Ref. [13] for our numerical studies, our conclusions are generic and rely on features that are common to all such approaches. Some recent form factor data that appeared after the fit of Ref. [13] are incorporated in the discussions of Secs. V and VI and support our numerical results.

II. SPECTRAL REPRESENTATION OF TRANSVERSE DENSITIES

The matrix element of the vector current operator between nucleon states with four–momenta p_1 and p_2 is parametrized by two functions of the invariant momentum transfer $t \equiv (p_2 - p_1)^2 < 0$, the Dirac and Pauli form factors, $F_1(t)$ and $F_2(t)$; see Ref. [14] for conventions and basic properties. The Dirac form factor at zero
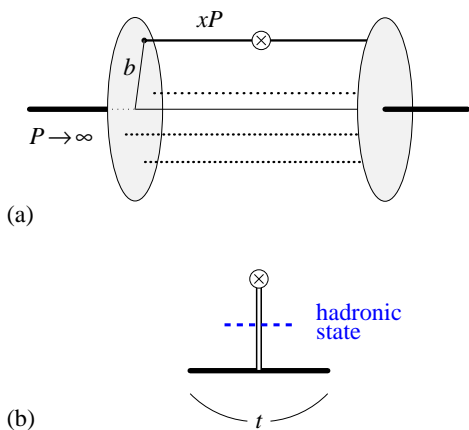
FIG. 1: (Color online) (a) Partonic interpretation of the transverse charge density. (b) Singularities of the timelike form factor resulting from transitions to hadronic intermediate states.

momentum transfer is normalized to the total charge of the nucleon,

$$F_1^p(0) = 1, \qquad F_1^n(0) = 0. \qquad (1)$$

Experimental knowledge of the nucleon form factors at spacelike momentum transfer is reviewed in Ref. [14]; for a discussion of the most recent data see e.g. Ref. [15].

The transverse charge densities of the nucleon are defined as the two–dimensional Fourier transform of the Dirac form factors

$$\rho^{p,n}(b) \equiv \int \frac{d^2\Delta}{(2\pi)^2} e^{-i(\Delta b)} F_1^{p,n}(t = -\Delta^2) \qquad (2)$$

$$= \int_0^\infty \frac{d\Delta}{2\pi} \Delta J_0(\Delta b) F_1^{p,n}(t = -\Delta^2), \qquad (3)$$

where $\Delta \equiv |\Delta|$ and $b \equiv |b|$. They have a simple interpretation in the infinite–momentum frame, where the nucleon is moving fast in the "longitudinal" direction and receives a momentum transfer Δ in the "transverse" direction. In this frame the coordinate b measures the distance from the transverse center of momentum of the nucleon, and the functions $\rho^{p,n}(b)$ describe the transverse spatial distribution of electric charge with normalization $\int d^2b \, \rho^{p,n}(b) = 1, 0$. As emphasized in Ref. [2], they are proper densities and can be expressed as the overlap integrals of the light–cone wave functions with the same momentum and particle number. More generally, they correspond to the x–integral of the impact parameter–dependent valence quark densities in the nucleon, which are defined as the Fourier transform of the diagonal GPDs and describe the densities of quarks minus antiquarks with respect to longitudinal momentum fraction x and transverse position b [10] (see Fig. 1a). Extensive numerical studies of the transverse charge densities have been performed using empirical parametrizations of the proton and neutron form factor data at space-

like momentum transfers; see Ref. [9] for a recent summary and analysis of the uncertainties.

The nucleon form factors are analytic functions of the invariant momentum transfer t, with singularities (branch cuts, poles) on the positive real axis. Assuming an asymptotic power behavior as $F_1(t) \sim |t|^{-2}$, as expected from perturbative QCD (with logarithmic modifications) and consistent with present experimental data, the Dirac form factor satisfies a dispersion relation

$$F_1^{p,n}(t) = \int_{4m_\pi^2}^\infty \frac{dt'}{t' - t - i0} \frac{\operatorname{Im} F_1^{p,n}(t')}{\pi}. \qquad (4)$$

It expresses the form factor in terms of its imaginary part on the principal cut in the physical sheet at $t > 4m_\pi^2$, also referred to as the spectral function. Physically, the singularities in the form factor at $t > 0$ correspond to the transition of a timelike virtual photon to a hadronic state coupling to a nucleon–antinucleon ($N\bar{N}$) pair (see Fig. 1b). Most of the states of interest, such as the vector mesons ρ and ω and their first excitations, lie below the $N\bar{N}$ threshold $t = 4m_N^2 = 3.5\,\mathrm{GeV}^2$, where the spectral functions cannot be measured directly in conversion experiments. However, theoretical methods can be used to constrain the spectral functions in the unphysical region; details will be given in Secs. III and IV below. Supplemented with such information and additional assumptions about the asymptotic behavior, the dispersion relations Eq. (4) have been used to fit nucleon form factor data in the spacelike region and extract information about the spectral functions [13, 16].

A new perspective on nucleon structure can be gained by combining the dispersion representation of form factors with the concept of transverse charge densities. Substituting Eq. (4) in Eq. (2) and carrying out the Fourier integral, one obtains the transverse charge density as a dispersion integral over the imaginary part of the Dirac form factor in the timelike region [8]

$$\rho^{p,n}(b) = \int_{4m_\pi^2}^\infty \frac{dt}{2\pi} K_0(\sqrt{t}b) \frac{\operatorname{Im} F_1^{p,n}(t+i0)}{\pi}. \qquad (5)$$

This spectral representation of the transverse density has several interesting properties. First, thanks to the exponential drop–off of the modified Bessel function K_0 at large arguments,

$$K_0(\sqrt{t}b) \sim [\pi/(2\sqrt{t}b)]^{1/2} e^{-\sqrt{t}b} \qquad (\sqrt{t}b \gg 1), \qquad (6)$$

the dispersion integral converges exponentially at large t, in contrast to the power–like convergence of the integral for the form factor, Eq.(4). This greatly reduces the sensitivity to the high–energy region where the spectral function is poorly known. As an aside, we note that use of a subtracted dispersion relation in Eq. (2) would lead to an expression for $\rho(b)$ which differs from Eq. (5) only
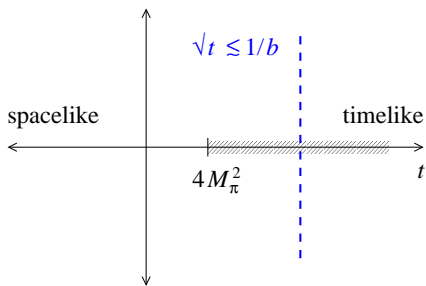
FIG. 2: (Color online) The "filtering" property of the spectral representation of the transverse charge density, Eq. (5). The dispersion integral extends over the cut of the form factor in the timelike region, $t > 4m_\pi^2$. Because of the weighting with $K_0(\sqrt{t}b)$ only energies of the order $\sqrt{t} \lesssim 1/b$ in the spectral function are effectively sampled in the integral.

by a term $\propto \delta^{(2)}(\boldsymbol{b})$; subtractions therefore have no influence on the dispersion result for the transverse density at finite b. In this sense the representation Eq. (5) is similar to the Borel transform used to eliminate polynomial terms in QCD sum rules [17].

Second, the transverse distance provides an external parameter which allows one to "filter out" a certain energy region in the spectral function. Because of the weighting with the kernel $K_0(\sqrt{t}b)$ in Eq. (5) the dominant contribution to the integral for a given b comes from energies in a range $\sqrt{t} \lesssim 1/b$ (see Fig. 2). This statement is to be understood in the sense of an exponential filter: significant numerical suppression happens already at energies inside the range $\sqrt{t} \lesssim 1/b$, determining the overall magnitude of the resulting density; the important point is in the *relative* suppression of higher energies (see Ref. [18] for a detailed discussion). We shall use this property in the following to identify regions in b that are maximally sensitive to certain spectral regions of physical interest, such as the near–threshold region $t - 4m_\pi^2 \sim$ few m_π^2 and the vector meson region $t \sim m_{\rho,\omega}^2$. The effectiveness of this method depends, of course, on the actual distribution of strength in the spectral functions and will be studied by numerical analysis. More generally, this property will allow us to associate the nucleon's partonic structure in the transverse periphery with the well–known exchange mechanisms in the nucleon form factors.

Third, the dispersion representation is the proper mathematical framework for discussing the asymptotic behavior of the transverse densities in the limit of large b and assess the uncertainties of the empirical densities in the region where they are exponentially small. It is well–known that the asymptotic behavior of the Fourier transform [or, for that matter, the Fourier–Bessel transform Eq. (3)] of a real function is determined by the singularities of that function in the complex plane, as can be shown by deformation of the integration contour of the Fourier integral. Parametrizations of the spacelike form factors in terms of rational functions of $Q^2 = -t$ [4, 19] generally have unphysical singularities

in the complex plane (e.g., pairs of complex conjugate poles with finite imaginary part) that lead to a qualitatively wrong asymptotic behavior of the Fourier integrals of Eqs. (2) and (3). The only way to ensure qualitatively correct asymptotic behavior of the charge density is to use form factor parametrizations with the proper analyticity, as provided by the dispersion representation of Eq. (4). In this case the Fourier integral over spacelike t becomes equivalent to the dispersion integral over timelike t, Eq. (5), and may be evaluated directly in this way. With the proper asymptotic form ensured by the correct position of the singularities, one may then estimate the numerical uncertainty of the large–b densities from the uncertainty of the spectral strength at low t [39].

For theoretical analysis it is convenient to consider the isovector and isoscalar combinations of form factors and the corresponding transverse charge densities [40]

$$F_1^{V,S}(t) \;\equiv\; \tfrac{1}{2}[F_1^p(t) \mp F_1^n(t)], \qquad (7)$$

$$\rho^{V,S}(b) \;\equiv\; \tfrac{1}{2}[\rho^p(b) \mp \rho^n(b)], \qquad (8)$$

which are normalized such that

$$F^{V,S}(0) \;=\; \int d^2b \, \rho^{V,S}(b) \;=\; 1/2. \qquad (9)$$

Because they involve t–channel states of isospin 1 and 0, respectively, the two combinations have very different spectral functions. In the following we discuss the spectral analysis of the transverse charge densities separately for the isovector and isoscalar channels, returning to the proton and neutron densities in Sec. V.

III. ISOVECTOR CHARGE DENSITY

The spectral function of the isovector nucleon form factor has been studied extensively in the literature and is under good theoretical control up to squared energies $t \sim 1\,\text{GeV}^2$. Because the isovector current couples to two pions, the threshold in this channel is at $t = 4\,m_\pi^2$. One can identify three distinct regions of the spectral function. At energies $t - 4\,m_\pi^2 \sim$ few m_π^2 the spectral function is governed by the universal threshold behavior implied by soft–pion dynamics and can be calculated in a model–independent manner. The traditional approach is to use dispersion theory to calculate the $\pi\pi \to N\bar{N}$ amplitude near threshold, taking care to include the effect of a branch cut singularity on the unphysical sheet close to $t = 4\,m_\pi^2$ [20, 21]. Another approach is through chiral perturbation theory with relativistic nucleons, which naturally implements the correct analytic structure of the soft–pion amplitudes [22, 23]. At somewhat higher energies, $t \lesssim 50\,m_\pi^2$, the spectral function is still saturated by the $\pi\pi$ channel, but rescattering effects play an important role away from threshold. In this region one can use elastic unitarity to calculate the spectral function in terms of the measured $\pi\pi$ phase shifts, which are dominated by the ρ resonance [20, 21]. At even higher ener-

gies, $t \gtrsim 50\,m_\pi^2$, the number of possible hadronic channels makes it impractical to calculate the spectral function from hadronic dynamics. However, it is constrained theoretically by the integral relations for the isovector charge (form factor at $t = 0$) and Dirac charge radius (derivative of the form factor at $t = 0$) following from the dispersion integral Eq. (4), as well as the requirement that the spacelike form factor drop faster than $|t|^{-1}$ at large momenta (superconvergence relation). In this energy region one may use a series of poles as an effective parametrization of the hadronic continuum, with the understanding that only their collective behavior, not the individual masses and coefficients, carry physical significance. Thus, in Ref. [13] the isovector spectral function is parametrized as

$$\mathrm{Im}\, F_1^V(t) \;=\; F_1^V(t)_{\pi\pi} \;+\; \sum_{i}^{n} a_i^V \delta(t - m_i^2), \quad (10)$$

where $F_1^V(t)_{\pi\pi}$ is the dispersion–theoretical result in the $\pi\pi$ channel, covering the near–threshold and ρ meson region, and the poles parametrize the effective continuum; the values of the parameters can be found in the quoted article. In the superconvergence (SC) fit of Ref. [13] the highest–mass singularity is actually parametrized as a broad resonance; this has practically no effect on our study of charge densities in the nucleon's periphery, as will be explained in the following. Figure 3 shows the empirical spectral function in the three different regions. For illustration we have chosen here $10\,m_\pi^2$ as the upper boundary of the near–threshold region; alternative choices will be discussed below, and our conclusions do not depend on the precise value.

Using this parametrization of the spectral function we can now quantify how much the different energy regions contribute to the isovector charge density at a given b. The results are summarized in Fig. 4. Plot (a) shows the exponential fall–off of the various contributions to $\rho^V(b)$ on a logarithmic scale. Plot (b) shows the radial density $2\pi b \rho^V(b)$ on a linear scale; the integral of the total radial density, given by the area under the sum of the curves, is the total isovector charge, $1/2$. The results show several interesting features. First, the near–threshold region $4\,m_\pi^2 < t < 10\,m_\pi^2$ is numerically important only at very large distances $b \gtrsim 2\,\mathrm{fm}$; see Fig. 4a. At smaller distances it is simply overwhelmed by the contribution of the ρ meson region, which has a faster exponential decay but a much larger coefficient. This confirms the conclusion of Ref. [8], that the chiral component in the nucleon's transverse charge density becomes clearly visible only at distances $b > 2\,\mathrm{fm}$. We note that the precise upper boundary of the near–threshold region is a matter of definition and depends on the requested accuracy of the chiral expansion for the spectral function. For $t < 10\,m_\pi^2$ the leading–order chiral result accounts for more than half of the dispersion result (see Appendix A and Fig. 10). However, it is not possible to substantially modify our conclusion by varying this value within
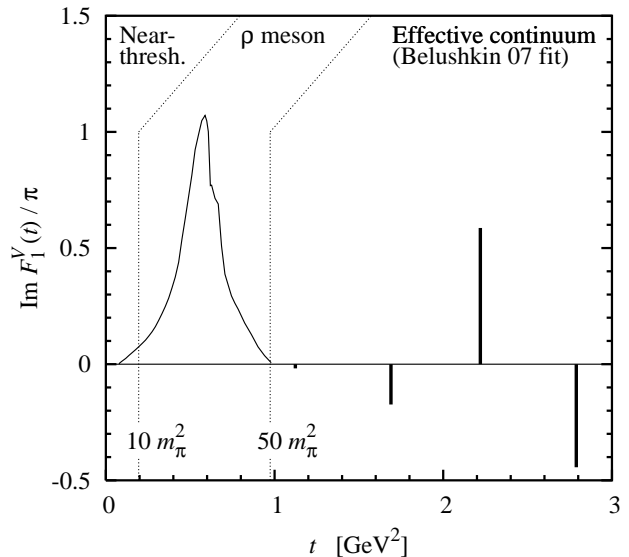

FIG. 3: Spectral function of the isovector nucleon Dirac form factor $\mathrm{Im}\,F_1^V(t)/\pi$ in the parametrization of Ref. [13]. The dotted lines indicate the boundaries of the three spectral regions discussed in the text: Near–threshold region $4\,m_\pi^2 < t < 10\,m_\pi^2$; ρ meson region, $10\,m_\pi^2 < t < 50\,m_\pi^2$; effective continuum region $t > 50\,m_\pi^2$. The solid line shows the dispersion theory result for the $\pi\pi$ contribution in the near–threshold and ρ meson regions. The spikes indicate the delta functions parametrizing the effective continuum; their absolute height is not drawn to scale, but the relative heights reflect the ratio of coefficients determined in the SC fit [13].

reasonable bounds: a change from $t = 10\,m_\pi^2$ to $15\,m_\pi^2$ would give a near–threshold contribution to $\rho^V(b)$ that is 1.7 times larger at $b = 2\,\mathrm{fm}$, which would have only a minor effect on the comparison with the ρ region on the logarithmic scale of Fig. 4a. The important point here is that for any choice of boundary our approach allows us to quantify unambiguously how much the region thus defined contributes to the transverse density.

Second, over a wide range of intermediate distances $0.5 \lesssim b \lesssim 1.5\,\mathrm{fm}$ the isovector transverse charge density is dominated by the ρ meson mass region; the high–mass continuum contribution reaches only -12% of the ρ at $b = 0.5\,\mathrm{fm}$ and is substantially smaller at larger b. The region $b \sim 1\,\mathrm{fm}$, where the near–threshold contribution is equally small, represents the cleanest case of "vector dominance" in the transverse charge density. Determination of the nucleon's transverse density in this region — by reconstructing it from spacelike form factor data, or through theoretical calculations — would thus provide unique information on the ρ meson contribution to the spectral function and thus its coupling to the nucleon. Note that the dispersion representation Eq. (5) allows us to both maximize the sensitivity to the ρ meson mass region and to quantify the corrections to vector dominance in a model–independent manner.
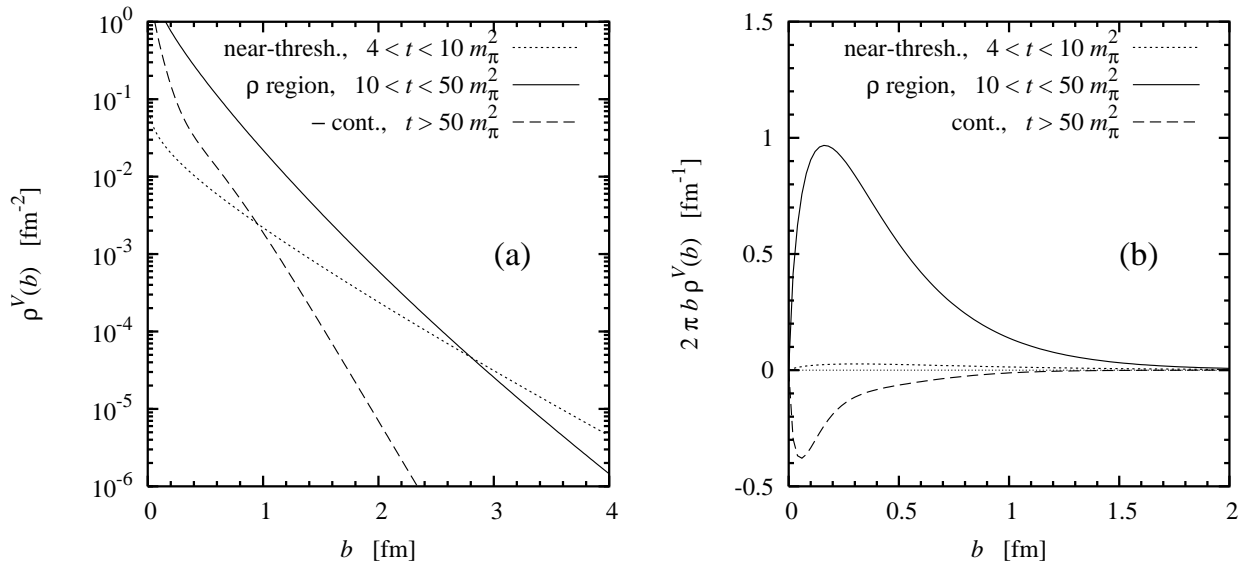
Third, the effective continuum contribution to the

FIG. 4: Contribution of different energy regions in the spectral function (cf. Fig. 3) to the isovector charge density in the nucleon, $\rho^V(b)$, calculated with the parametrization of Ref. [13] (SC fit). (a) Density $\rho^V(b)$ on a logarithmic scale. (b) Radial density $2\pi b \rho^V(b)$ on a linear scale. Dotted lines: Near–threshold region $4\,m_\pi^2 < t < 10\,m_\pi^2$. Solid lines: ρ meson region $10\,m_\pi^2 < t < 50\,m_\pi^2$. Dashed lines: Effective continuum $t > 50\,m_\pi^2$; this contribution is negative and shown with reversed sign in the logarithmic plot (a).

charge density remains relatively small down to distances as small as $b \sim 0.3$ fm. This happens because of the low spectral strength in the region immediately above the ρ, $1.0 < t < 1.4\,\mathrm{GeV}^2$, and the substantial cancellations between the higher–mass poles in the parametrization [13] (see Fig. 3). Whether the nucleon spectral function in the region above the ρ could at least partly be explained by the ρ' resonances seen in the $\pi\pi$ channel is an interesting question which cannot be answered from form factor fits alone. We note that the $e^+e^- \to \pi\pi$ data clearly show a broad ρ' resonance at $1.4\,\mathrm{GeV}$ that interferes destructively with the ρ and results in a vanishing $\pi\pi$ strength at $t \sim 1.2\,\mathrm{GeV}^2$ (see Ref. [24] and references therein), in qualitative agreement with the empirical strength distribution found in the nucleon form factor fit [13].

In the SC fit of Ref. [13] the highest–mass pole in Eq. (10) was actually replaced by a contribution to the form factor of the form

$$a_n^V (m_n^2 - t)/[(m_n^2 - t)^2 + \Gamma_n^2], \qquad (11)$$

with Γ_n comparable to m_n^2, mimicking the effect of a broad resonance. As it stands, this term has poles in the complex plane away from the real axis, at $t = m_n^2 \pm i\Gamma_n$, and cannot be regarded as a contribution to the spectral function. However, as can be seen by calculating the charge density from the Fourier integral Eq. (3) over spacelike momentum transfers, the contribution of this term to the isovector density is very small at all but the shortest distances, $< 2\%$ at $b > 0.1$ fm and $\ll 1\%$ at $b > 0.5$ fm, and we can safely neglect it in our study of the nucleon's periphery. The same applies to the highest–mass pole in the isoscalar density considered in Sec. IV.

In Ref. [8] we studied the question at what distances the isovector transverse charge density is dominated by chiral dynamics in a theoretical approach, by comparing the chiral perturbation theory result for the transverse density at $b \sim 1/m_\pi$ with the non–chiral density modeled by elementary ρ meson exchange. An interesting question is how the theoretical approach of Ref. [8] relates to the present study of the transverse densities using empirical spectral functions. This is explained in Appendix A, where we summarize how well the empirical isovector spectral function in the different regions is reproduced by the theoretical models used in Ref. [8]. Overall, the present analysis with empirical spectral functions fully confirms our earlier conclusion that the chiral component becomes numerically dominant only at distances $b \gtrsim 2$ fm, contradicting naive expectations that the charge densities at $b \gtrsim 1$ fm could be attributed to the nucleon's "pion cloud."

IV. ISOSCALAR CHARGE DENSITY AND ITS UNCERTAINTY

The isoscalar spectral function at low energies behaves very differently from the isovector one, and comparatively little is known about it from first principles. The lowest hadronic state in the isoscalar channel allowed by quantum numbers is the 3π state. The non-resonant 3π contribution near threshold was estimated using heavy–baryon chiral perturbation theory [25] and found to be roughly two orders of magnitude smaller than the 2π contribution in the isovector channel; it therefore plays
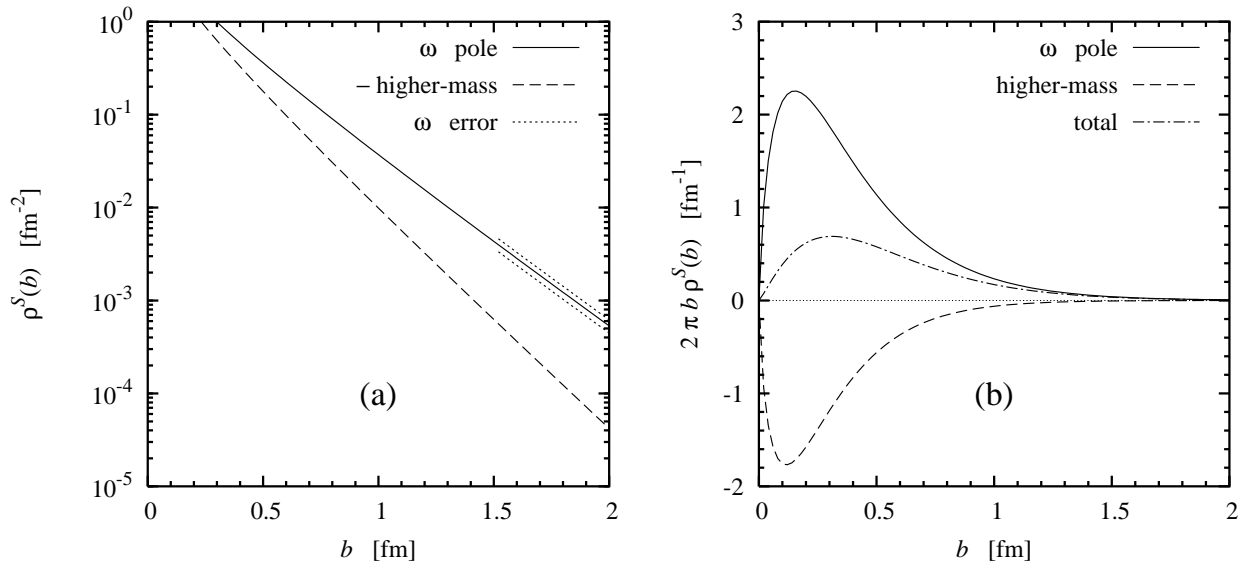
FIG. 5: Contribution of different energy regions in the spectral function to the isoscalar charge density in the nucleon, $\rho^S(b)$, calculated with the parametrization of Ref. [13] (SC fit). (a) Density $\rho^S(b)$ on a logarithmic scale. Solid line: ω meson pole. Dashed line: Higher–mass states $t > 1\,\mathrm{GeV}^2$, including both identified hadronic states ($K\bar{K}, \rho\pi$) and the effective continuum (this contribution is negative and shown with reversed sign). Dotted lines: Error band of the ω contribution, giving approximately the uncertainty of the total isoscalar density at $b > 1.5\,\mathrm{fm}$. (b) Radial density $2\pi b\rho^S(b)$ on a linear scale. Solid line: ω meson pole. Dashed line: Higher–mass states $t > 1\,\mathrm{GeV}^2$. Dot–dashed line: Total.

no role in the transverse charge density at the distances $b \sim 2 - 3\,\mathrm{fm}$ of interest here (cf. Fig. 4a). The strength in the 3π channel is overwhelmingly concentrated in the ω resonance at $m_\omega = 0.782\,\mathrm{GeV}$, whose width can be neglected for our purposes. At energies $\sqrt{t} \gtrsim 1\,\mathrm{GeV}$ other hadronic channels come into play. The $K\bar{K}$ contribution was computed using dispersion theory [26, 27] and exhibits the ϕ resonance at 1.02 GeV, very close to threshold; in contrast to $\pi\pi$ in the isovector channel there is no enhancement of the strength to the left of the resonance. In the parametrization of Ref. [13] the entire $K\bar{K}$ strength is described by an effective pole at the ϕ mass. Additional strength in this region is expected to come from the $\pi\rho$ continuum, which was found to be sizable in the context of the Bonn–Jülich meson exchange model of the NN interactions [28]. This contribution is again parametrized by an effective pole. We emphasize that the details of the theoretical estimates of these explicit higher–mass contributions are ultimately not essential for the accuracy of the parametrization of the spectral function in Ref. [13], as these states have masses of the same order as the effective continuum poles, whose strength is determined by the fit to the form factor data.

For the purpose of our analysis, we divide the empirical isoscalar spectral function into the ω pole, which is the analogue of the ρ in the isovector channel and accounts for the entire strength at energies $\sqrt{t} < 1\,\mathrm{GeV}$, and a "rest" of higher–mass states, about whose nature we remain agnostic at this point. The respective contributions to the isoscalar transverse charge density are shown in Fig. 5. One sees that the relative contribution

from higher–mass states is substantially larger than in the isovector density, amounting to -27% of the ω at $b = 1\,\mathrm{fm}$. Vector dominance at intermediate distances is therefore realized not as perfectly as in the isovector charge density. However, because of the absence of a nonresonant contribution below the ω mass, in the isoscalar case one has the option to go to larger distances to maximize the vector meson contribution: at $b = 2\,\mathrm{fm}$ the contribution from higher–mass states has dropped to -8% of the ω. Thus, it is possible to realize "vector meson dominance" in the isoscalar charge density as well.

In view of the paucity of theoretical information in the isoscalar sector, it is worthwhile to consider the uncertainty of the empirical isoscalar transverse density at large b. In the region where it is dominated by the ω contribution its uncertainty is essentially determined by the accuracy with which the coefficient of the ω pole can be determined from dispersion fits to the isoscalar form factor. The analysis of Ref. [13] quotes an uncertainty of $\pm 16\%$ for the ω coefficient; we can therefore ascribe a relative uncertainty of this magnitude to the isoscalar charge density at $b > 1.5\,\mathrm{fm}$, where the ω accounts for more than 80% of the total density (see Fig. 5). (An even larger range of ωNN couplings is quoted in Ref. [29]; however, that analysis uses a more restrictive form factor fit than the one of Ref. [13].) At smaller values of b the contribution from higher–mass poles can no longer be neglected and correlations between the errors of the coefficients of the various poles become important in estimating the error of the total charge density; unfortunately, this information is not provided in the fit of Ref. [13].
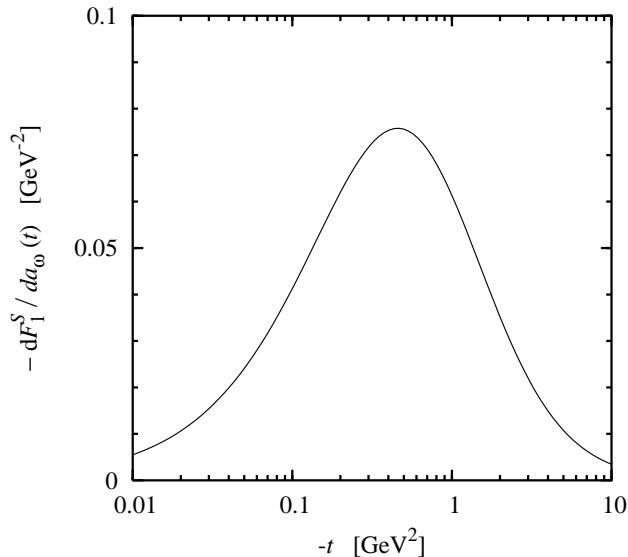
FIG. 6: Sensitivity of the pole fit to the isoscalar form factor, Eq. (12), to the ω coefficient a_ω. The curve shows the derivative of the form factor with respect to a_ω after the constraints Eqs. (13) and (14) were used to eliminate two of the other parameters. Here $N = 3$, and the pole masses are those of the SC fit of Ref. [13].

Altogether, we see that there is considerable uncertainty in the isoscalar charge density at large b.

In order to determine more accurately the isoscalar transverse density in the nucleon's periphery it is obviously necessary to gain better knowledge of the coefficient of the ω pole in the isoscalar spectral function (or, equivalently, the ωNN coupling) from dispersion fits to spacelike form factor data. It is interesting to ask at what momentum transfers future form factor measurements would have the strongest impact on the determination of the ω coefficient. Naively one might think that, because the ω completely dominates the charge density at $b \gtrsim 2\,\text{fm}$, form factor data at $-t \lesssim \pi^2/(2\,\text{fm})^2 = 0.1\,\text{GeV}^2$ would be most useful to constrain the ω coefficient. However, it is data over a broad range of intermediate momentum transfers $-t \sim m_\omega^2$ that effectively determine the ω coefficient in the dispersion analysis. The reason lies in the nature of the spectral representation — the ω is the leading singularity, and all spacelike momenta in the range $-t \sim m_\omega^2$ are equally affected by the strength of this pole. To see this explicitly, let us consider a spectral representation of the isoscalar form factor as an ω pole and a sum of $n - 1$ higher–mass poles [13, 16]

$$ F_1^S(t) \;=\; \frac{a_\omega}{m_\omega^2 - t} \;+\; \sum_{i=2}^{n} \frac{a_i^S}{m_i^2 - t}. \qquad (12) $$

The coefficients are constrained by charge conservation

and the $|t| \to \infty$ asymptotic behavior of the form factor,

$$ F_1^S(0) \;=\; 1/2, \qquad (13) $$

$$ \lim_{|t| \to \infty} t\, F_1^S(t) \;=\; 0. \qquad (14) $$

The resulting linear relations allow one to express two coefficients in terms of the other $n - 2$. A value $n \geq 3$ is required to have sufficient flexibility in the fit and avoid artificial correlations between the behavior at small and large $|t|$. The fit of Ref. [13] effectively works with $n = 4$ [41]; that its highest–mass pole has a finite width, Eq. (11), is not important for our argument here. Figure 6 shows the derivative of the form factor parametrization Eq. (12) with respect to a_ω after the constraints Eqs. (13) and (14) were used to eliminate two of the other coefficients, for $n = 4$ and the mass values of Ref. [13] (the a_ω–derivative does not depend on the value of the remaining free coefficient but only on the position of the poles). The result clearly shows that the sensitivity to a_ω is broadly distributed over a range of momentum transfers $|t| \sim m_\omega^2$, suggesting that precise form factor measurements in this region would be most useful to constrain this parameter. A more accurate analysis of the impact of future form factor data on the determination of the large–b isoscalar densities, with account of experimental uncertainties and correlations between parameters, remains an interesting problem for further study.

V. PROTON AND NEUTRON CHARGE DENSITIES

Using the dispersion results for the isovector and isoscalar transverse densities we can construct the transverse charge densities in the proton and neutron, cf. Eq. (8). The results are shown in Fig. 7. The dispersion integral Eq. (5) with the spectral functions of Ref. [13] gives a peripheral charge density in the neutron that is clearly negative above $b \gtrsim 1.5\,\text{fm}$, and positive over a wide range of intermediate distances $b \sim 0.5 - 1.5\,\text{fm}$. A positive density at such distances was found previously in a Fourier analysis of the spacelike neutron form factor [2]. With the insights into the spectral composition of the transverse change densities from the studies of Secs. III and IV we can now explain this behavior of the neutron charge density from the t–channel point of view.

The negative charge density in the neutron at large distances arises because the spectral strength in the isovector channel starts at lower masses than in the isoscalar channel, namely $4m_\pi^2$ rather than m_ω^2. As a result, the isovector density has a slower exponential decay and becomes dominant in the $b \to \infty$ limit (note that $\rho^n = \rho^S - \rho^V$). This is a robust prediction of the dispersion approach, which is independent of the details of the parametrization of the spectral functions. Qualitatively, such large–distance behavior is consistent with the the picture of the neutron as a proton at the center and a negative pion in the cloud. However, the analysis of
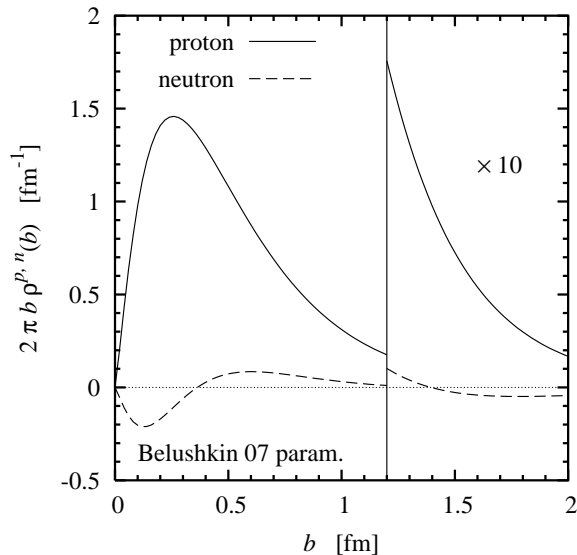
FIG. 7: Transverse charge densities in the proton (solid line) and neutron (dashed line) obtained from the dispersion integral Eq. (5) with the empirical spectral functions of Ref. [13].
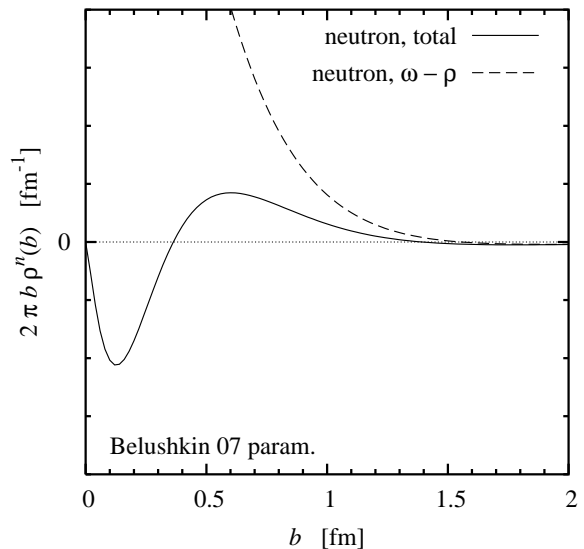

FIG. 8: Spectral composition of the transverse charge density in the neutron, as evaluated with the spectral functions of Ref. [13]. Solid line: Total dispersion result (cf. Fig. 7). Dashed line: Contribution from $\sqrt{t} < 1\,\text{GeV}$, given by the difference $\omega - \rho$ (here ρ includes the near–threshold region).

Sec. III shows that the chiral near–threshold region of the isovector spectral function becomes numerically dominant only at very large distances $\gtrsim 4\,\text{fm}$ (see Fig. 4a). At the distances of interest here, $b \sim 2\,\text{fm}$, the isovector density results rather from the broadly distributed strength in the ρ meson region. We conclude that non–chiral interactions still play an essential role in the transverse density at such distances. That the "pion cloud" is not yet dominant at $b \sim 2\,\text{fm}$ is also seen from the fact that the proton and neutron densities are still far from being equal and opposite in sign, because of the large isoscalar density arising from the ω.

The positive density in the neutron at intermediate distances $b \sim 1\,\text{fm}$ lies in the region where vector mesons give a prominent contribution to the isovector and isoscalar transverse densities; cf. Secs. III and IV. An interesting question is whether the positive charge density in the neutron could be explained solely on the basis of the vector meson region in the spectral functions, i.e., as the result of vector meson exchange in the form factor. To answer this question one needs to look in detail at the spectral composition of the neutron charge density in the region $b \sim 0.5 - 1.5\,\text{fm}$. Figure 8 shows the total neutron charge density obtained from the dispersion integral, as well as the result from the region $\sqrt{t} < 1\,\text{GeV}$, corresponding to the difference of the ω and ρ region of the isoscalar and isovector spectral functions, respectively (here the near–threshold region is included in the ρ; but its contribution is numerically small, see Fig. 4). One sees that the vector meson region alone does produce a positive neutron charge density; however, with the ωNN coupling of Ref. [13], this contribution is substantially larger than the full dispersion result. Higher–mass states, particularly in the isoscalar channel, are essential

for explaining the positive neutron charge density at the quantitative level.

In sum, our t–channel analysis shows that the precise value of the transverse charge density in the neutron at distances $b \sim 0.5 - 1.5\,\text{fm}$ is closely tied up with the question of the spectral strength in the isoscalar channel at masses $\sqrt{t} \sim 1\,\text{GeV}$. As shown in Sec. IV, the information on the transverse density in this region comes from form factor measurements over a broad range of intermediate momentum transfers $|t| \sim 0.1 - 1\,\text{GeV}^2$ (see Fig. 6 for the isoscalar component). Accurate measurements of the neutron form factor at these momentum transfers may thus considerably improve our knowledge of the isoscalar spectral function. Because of the potential contribution from mesons containing strange quarks $(K\bar{K}, \phi)$, this question is of interest also for the determination of the strangeness content of the nucleon; see Ref. [29] and references therein.

The transverse charge density in the neutron at large b was recently studied by evaluating the Fourier transform of the spacelike form factor Eq. (3) [30], using an updated version of the Friedrich–Walcher form factor parametrization [4] that includes recent data from the BLAST [31] and Jefferson Lab Hall A experiments [32]. For $b < 2\,\text{fm}$ their Fourier result agrees well with the neutron density obtained from the dispersion integral Eq. (5) with the spectral functions of Ref. [13], with a maximum discrepancy of $\sim 20\%$ at $b = 1.7\,\text{fm}$. At $b > 2.4\,\text{fm}$ the Fourier result of Ref. [30] becomes positive, in contradiction to the robust prediction of the dispersion approach (see above). This behavior of the Fourier transform may be a consequence of the fact that the spacelike form fac-

tor fit of Ref. [4] uses a higher–order rational function with unphysical singularities in the complex t–plane; cf. the discussion in Sec. II.

VI.   IMPLICATIONS FOR PARTONIC STRUCTURE

The transverse densities obtained from the dispersion representation of the nucleon form factors provide interesting insight into the nucleon's partonic structure. Here we would like to point out several implications that can be stated in a model–independent manner.

For the partonic interpretation of our results it is convenient to extract the transverse densities of u and d valence quarks in the proton, defined as the integral over x of the impact parameter–dependent valence quark distributions:

$$\rho_u(b) \equiv \int_0^1 dx\, u_{\text{val}}(x, b), \tag{15}$$

$$u_{\text{val}}(x, b) \equiv u(x, b) - \bar{u}(x, b) \quad \text{etc.}; \tag{16}$$

the latter reproduce the usual valence quark distributions upon integration over the transverse plane,

$$\int d^2 b\, u_{\text{val}}(x, b) = u_{\text{val}}(x) \equiv u(x) - \bar{u}(x) \quad \text{etc.} \tag{17}$$

The transverse densities of u and d valence quarks are related to the isoscalar and isovector charge densities by

$$\rho_{u,d}(b) = 3\rho^S(b) \pm \rho^V(b) \tag{18}$$

and normalized such that $\int d^2 b\, \rho_{u,d}(b) = 2, 1$. Figure 9 shows the ratio of d– and u–quark transverse valence quark densities, $\rho_d(b)/\rho_u(b)$, as obtained from the dispersion integral Eq. (5) evaluated with the spectral functions of Ref. [13]. The numerical result exhibit several interesting features. In the limit of large transverse distances we expect that

$$\rho_d(b)/\rho_u(b) \rightarrow -1 \qquad (b \rightarrow \infty). \tag{19}$$

In the t–channel (or exchange mechanism) view this should happen because at asymptotically large b the isovector charge density due to chiral two–pion exchange near threshold should become dominant; see Secs. III and A. In the s–channel (or partonic) view the transverse density at such distances should result from configurations in the proton's light–cone wave function corresponding to a neutron at the center and a peripheral π^+, which contribute to the u and $\bar{d}$ distributions in the proton. The numerical results show that the ratio becomes negative at $b > 2.5$ fm but is still far from -1, reaffirming our earlier conclusion that the chiral component becomes numerically dominant only at substantially larger distances.

Over a broad range of intermediate transverse distances the d/u valence quark density ratio in Fig. 9 is

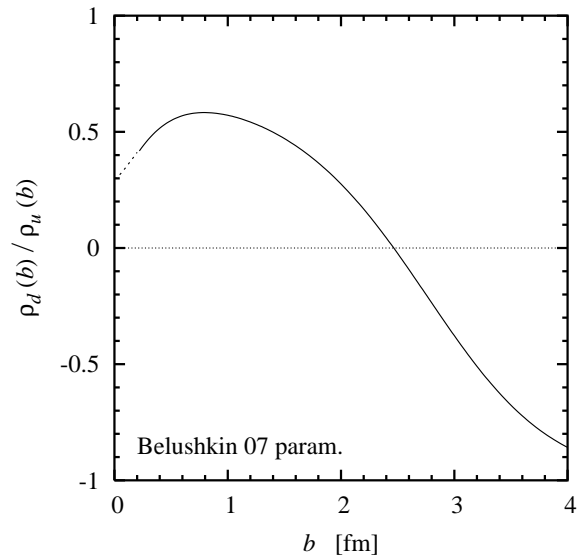$$\rho_d(b)/\rho_u(b) \approx 1/2 \qquad (0.2\,\text{fm} \lesssim b \lesssim 1.6\,\text{fm}). \tag{20}$$

FIG. 9: Ratio of d– and u–quark transverse valence quark densities in the proton, $\rho_d(b)/\rho_u(b)$, as a function of b, as obtained from the dispersion integral Eq. (5) evaluated with the spectral functions of Ref. [13].

This is the value one would obtain in a generic mean–field picture of the nucleon, in which constituent u– and d–quarks in the rest frame move approximately independently on identical orbitals; the detailed manner in which these effective degrees of freedom project on the quark partons in the infinite–momentum frame is irrelevant here, as it would be common to the u– and d–flavors and cancel in the ratio Eq. (20). For example, the $SU(6)$ quark model gives $d_{\text{val}}(x)/u_{\text{val}}(x) = 1/2$ even with relativistic corrections (see Ref. [33] and references therein); the same would be true for the b–dependent valence quark distributions Eq. (16), whose integral over x gives the transverse densities Eq. (15). In this sense, Eq. (20) offers model–independent evidence of an approximate mean–field picture of the nucleon's valence quark structure at distances $b \sim 1$ fm. In the t–channel view this region of distances is governed by the vector mesons, albeit with a non–negligible contribution from higher–mass states in the isoscalar channel. Exploring this duality between valence quark structure and vector meson exchange in dynamical models of the nucleon would be an interesting problem for further study.

The same conclusion could in principle be reached already from inspection of the proton and neutron charge densities in Fig. 7. The neutron density in the region $0.3 < b < 1.5$ fm is substantially smaller than the proton one; in the mean–field picture the former would be zero. The advantage of using the ratio $\rho_d(b)/\rho_u(b)$ is that it eliminates much of the non–trivial b–dependence on the bound–state structure in this region.

Finally, at even smaller distances, $b < 0.2$ fm, the charge density ratio obtained from the dispersion representation of Ref. [13] drops significantly below the mean–

field value of $1/2$ (see Fig. 9) [42]. At such values of b it is possible that part of the proton charge density results from partonic configurations in which the active quark carries large momentum fraction $x \sim 1$, while the spectators are restricted to substantially smaller values [34]. (The variable b measures the distance of the active parton from the transverse center–of–mass of the nucleon, see Fig. 1a [10]. For $x \to 1$ the center–of–mass coincides with the position of the active parton, whence such configurations contribute to the density at $b \to 0$ independently of their physical transverse size; see Ref. [18] for a detailed discussion.) The observed behavior of $\rho_d(b)/\rho_u(b)$ is consistent with a decreasing ratio of d and u valence quark distributions at large x,

$$d_{\mathrm{val}}(x)/u_{\mathrm{val}}(x) \ \ll \ 1 \qquad (x \to 1). \tag{21}$$

Experimental information on this ratio at large x is dependent on theoretical corrections to nuclear binding effects in measurements with nuclear targets, which are the subject of on–going research; new data are expected with the 12 GeV Upgrade of Jefferson Lab [35]. A joint analysis of elastic form factors and large–x inclusive scattering data could explore the properties of large–x configurations in the nucleon's partonic wave function more effectively than either class of observables alone.

We note that at distances $b < 0.2$ fm the proton and neutron charge densities defined by Eqs. (2) and (3) are sensitive to the spacelike form factors at high momentum transfers where experimental information is limited, especially for the neutron. In particular, the u– and d– quark densities at $b = 0$ can be obtained from the ordinary (not Fourier) integrals of the spacelike form factors as

$$\rho_{u,d}(b = 0) \ = \ \int_0^\infty \frac{dQ^2}{4\pi}\, F_{1u,d}(t = -Q^2), \tag{22}$$

where $F_{1u} \equiv 2F_1^p + F_1^n$ and $F_{1d} \equiv 2F_1^n + F_1^p$ are the u– and d–quark contributions to the form factor. A recent analysis [15] including the neutron data from the Jefferson Lab Hall A experiment [32] extracted the u– and d–quark Dirac form factors up to $Q^2 = 3.4\,\mathrm{GeV}^2$. Integration of these data, assuming extrapolation into the unmeasured high–Q^2 region by a rational fit with a leading $1/Q^4$ behavior, gives a ratio $\rho_d(0)/\rho_u(0) \approx 0.35$, somewhat larger than the value 0.3 obtained from Ref. [13] (see Fig. 9), but still substantially below $1/2$. We note that at $b > 0.2$ fm the charge densities obtained from these data are in good agreement with those obtained from the dispersion fit of Ref. [13]. With the 12 GeV Upgrade of Jefferson Lab the neutron's Dirac form factor will be measured up to $Q^2 \sim 8\,\mathrm{GeV}^2$ [35], substantially reducing the uncertainties in the u– and d–quark densities at small b.

VII. SUMMARY AND OUTLOOK

The dispersion approach to transverse densities allows one to formulate the concept of vector dominance in the nucleon form factors in a manner which is fully quantitative and consistent with QCD. Extraction of the transverse densities in the region $b \sim 1$ fm can provide unique information on the ρ meson's coupling to the nucleon. It also affords a model–independent definition that could in principle serve as a basis for calculating this hadronic coupling using non–perturbative QCD methods, such as lattice calculations.

The spectral analysis of transverse densities at intermediate distances $b \sim 1$ fm suggests an interesting connection between vector dominance and the valence quark structure of the nucleon. Such duality might be realized in a relativistic constituent quark picture, where the leading singularity "seen" by the current is at a mass $\sqrt{t} = 2m_{\mathrm{const}} \approx m_\rho$. An effective dynamics of chiral constituent quarks at a low resolution scale appears as a result of the spontaneous breaking of chiral symmetry in QCD. Exploring this connection in explicit dynamical models would be an interesting problem for further study.

Generally, the dispersion representation Eq. (4) provides the proper mathematical framework for studying transverse densities at distances $b \gtrsim 1$ fm. Its analyticity ensures the correct asymptotic behavior of the density, and the exponential fall–off of the different contributions is encoded already in the position of the singularities. It thus represents a valuable tool for studying peripheral nucleon structure using empirical or theoretical methods. Dispersion fits to the spacelike nucleon form factors therefore have a special significance and should be given high priority as a method of data analysis [13]. Such fits should be updated as new data become available, particularly with the 12 GeV Upgrade of Jefferson Lab that will cover the high–Q^2 region with high precision. One should also explore improved parametrizations of the spectral functions in the high–mass region that satisfy QCD constraints and respect the analytic properties of the form factor.

Neutron form factor data are of particular importance for extracting the ωNN coupling and, indirectly, the coupling of higher–mass states in the isoscalar channel possibly related to the nucleon's strangeness content. Our estimates show that these objectives require accurate measurements over a broad range of intermediate momentum transfers $|t| \sim 0.1 - 1\,\mathrm{GeV}^2$ rather than exceptionally large or small values.

A similar spectral analysis could be performed for the nucleon's Pauli form factor, whose partonic representation is related to the angular momentum of partons in the light–cone wave function; such analysis is in progress. The approach described here could also be extended to the axial form factors, whose transverse representation constrains the quark helicity distributions in the nucleon.

Acknowledgments

Appendix A: Theoretical analysis of isovector charge density

In Ref. [8] we studied the question at what transverse distances the isovector charge density in the nucleon is dominated by the universal chiral dynamics that governs the long–range behavior of strong interactions. The large–b limit of the isovector charge density is determined by the threshold behavior of the spectral function near $t \to 4\,m_\pi^2$, corresponding to t–channel exchange of two soft pions, which can be analyzed in a model–independent manner within chiral perturbation theory [22, 23]. By comparing the calculated chiral contribution to the non–chiral density arising from zero–width ρ meson exchange we found that the former becomes numerically dominant only at distances $b \gtrsim 2\,\mathrm{fm}$. In this appendix we explain how the theoretical approach of Ref. [8] relates to the present dispersion analysis of the transverse densities, by showing how well, and in what sense, the theoretical approximations used in Ref. [8] reproduce the empirical spectral functions. This also allows us to address some questions concerning the quantitative comparison of "chiral" and "non–chiral" components of the transverse density that were not discussed in detail in Ref. [8], such as the role of higher–order chiral corrections, the finite width of the ρ, and the value of the ρNN coupling.

The one–loop chiral result for the isovector spectral function near threshold can be stated as [8]

$$\frac{\mathrm{Im}F_1^V(t+i0)}{\pi} = \frac{g_A^2(t-2m_\pi^2)^2}{4(4\pi f_\pi)^2 m_N \sqrt{t}}(X - \arctan X)$$
$$+ \frac{2(1-g_A^2)[k(t)]^3}{3(4\pi f_\pi)^2 \sqrt{t}}, \qquad (A1)$$

$$X \equiv 4m_N k(t)/(t-2m_\pi^2), \qquad (A2)$$

where $g_A = 1.26$ is the nucleon isovector axial coupling, $f_\pi = 93\,\mathrm{MeV}$ the pion decay constant, and

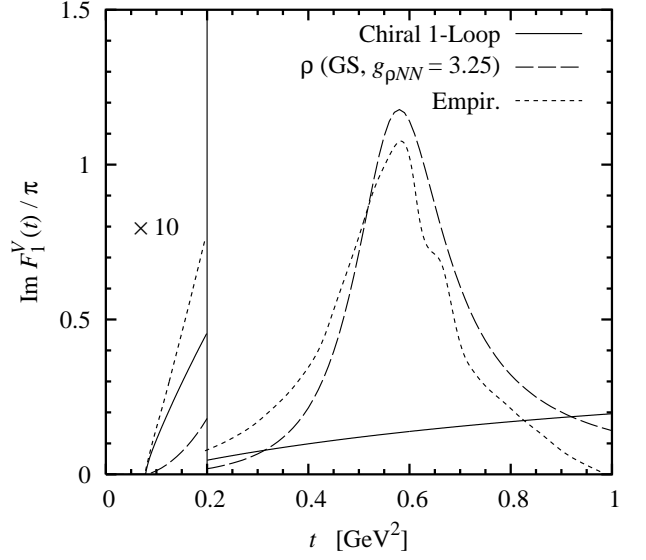$$k(t) \equiv \sqrt{t/4 - m_\pi^2} \qquad (A3)$$

FIG. 10: Comparison of theoretical approximations to the isovector spectral function with the empirical result of Ref. [21]. Solid line: Chiral one–loop result, Eq. (A1). Dashed line: ρ meson contribution [GS form Eq. (A10), $\Gamma_\rho = 0.15\,\mathrm{GeV}$] with $g_{\rho NN} = 3.25$ from the Bonn–Jülich model [37]. Dotted line: Empirical spectral function from dispersion analysis in the two–pion channel [21].

the t–channel center–of–mass momentum of the $\pi\pi$ system (here $t > 4\,m_\pi^2$). Equations (A1) and (A2) represent a compact approximation to the exact chiral 1–loop result with relativistic nucleons [22, 23] in which we omitted certain terms of order t/m_N^2 that become numerically important only at $t \sim 1\,\mathrm{GeV}^2$ and give negligible contributions to the charge density at large b. In Fig. 10 we compare our approximate expression Eq. (A1) with the empirical spectral density obtained from the dispersion analysis of Ref. [21], which represents an update of the classic result of Ref. [20]. One sees that the one–loop result gives a reasonable representation of the empirical spectral density near threshold, with the discrepancy reaching $\sim 50\%$ at $t \approx 10\,m_\pi^2 = 0.195\,\mathrm{GeV}^2$. Two–loop chiral corrections were studied in Ref. [23] and found to increase the value in this region by $\sim 20\%$. We emphasize that the chiral expression is physically meaningful only in the near–threshold region $t - 4m_\pi^2 \sim$ few m_π^2; its numerical value at larger t is shown for illustrative purposes only.

In Ref. [8] we approximated the ρ meson contribution to the isovector charge density using a zero–width pole. A simple theoretical model of the ρ meson contribution incorporating the finite ρ width and its energy dependence is the Gounaris–Sakurai (GS) form factor, obtained from an effective range expansion of the $\pi\pi$ scattering phase shift [36]. The spectral function of the resulting form factor $F_{\mathrm{GS}}(t)$, normalized to $F_{\mathrm{GS}}(0) = 1$, is of the form

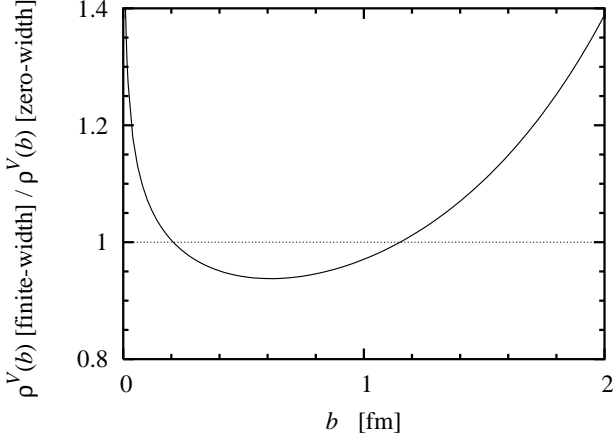$$\frac{\mathrm{Im}F_{\mathrm{GS}}(t+i0)}{\pi} = \frac{CB(t)}{\pi[A^2(t) + B^2(t)]}, \qquad (A4)$$

FIG. 11: Ratio of the isovector transverse charge densities $\rho^V(b)$ obtained from a finite–width ρ meson [GS form Eq. (A4), $\Gamma_\rho = 0.15\,\text{GeV}$] to the corresponding density for a zero–width pole. Both distributions are normalized to the same total charge.

with

$$
\begin{aligned}
A(t) &\equiv m_\rho^2 - t + (\Gamma_\rho m_\rho^2/k_\rho^3)\{k_\rho^2 h_\rho'(m_\rho^2 - t) \\
&\quad + [k(t)]^2\,[h(t) - h_\rho]\},
\end{aligned}
\tag{A5}
$$

$$
B(t) \equiv (m_\rho^2 \Gamma_\rho/\sqrt{t})[k(t)/k_\rho]^3,
\tag{A6}
$$

$$
\begin{aligned}
C &\equiv m_\rho^2 + (\Gamma_\rho m_\rho^2/k_\rho^3)[k_\rho^2 h_\rho' m_\rho^2 \\
&\quad + m_\pi^2 h_\rho - m_\pi^2/\pi],
\end{aligned}
\tag{A7}
$$

where Γ_ρ is the width parameter, $k(t)$ the t–channel $\pi\pi$ center–of–mass momentum Eq. (A3), $k_\rho \equiv k(m_\rho^2)$, and $h(t)$ denotes the auxiliary function

$$
h(t) \equiv \frac{2k(t)}{\pi\sqrt{t}}\ln\frac{\sqrt{t} + 2k(t)}{2m_\pi},
\tag{A8}
$$

with $h_\rho \equiv h(m_\rho^2)$ and $h_\rho' \equiv dh/dt(m_\rho^2)$. These expressions apply at $t > 4m_\pi^2$. In fact, the full complex form factor on the upper edge of the cut at $t > 4m_\pi^2$ is given by

$$
F_{\text{GS}}(t+i0) = \frac{C}{A(t) - iB(t)},
\tag{A9}
$$

and its values at $t < 4m_\pi^2$ can be obtained by proper analytic continuation of the expressions in Eqs. (A5), (A6), and (A8). One finds that the form factor is regular at $t = 0$, as should be [the apparent singularity from the $\sqrt{t}$ factors in Eqs. (A6) and (A8) cancels between the two terms in the denominator of Eq. (A9)] and is normalized to unity there. In Fig. 11 we compare the transverse charge density obtained from the finite–width spectral function Eq. (A4) et seq. ($m_\rho = 0.77\,\text{GeV}, \Gamma_\rho = 0.15\,\text{GeV}$) with that obtained in the zero–width approximation; both densities here are normalized to the same integral (total charge). One sees that the zero–width
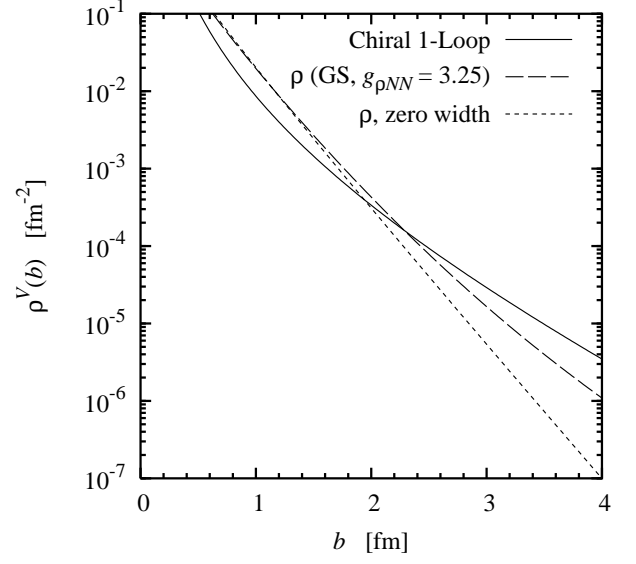

FIG. 12: Comparison of the transverse charge densities $\rho^V(s)$ resulting from the chiral and ρ meson approximations to the isovector spectral function (cf. Fig. 10). Solid line: Charge density from the one–loop chiral result Eq. (A1). Dashed line: Charge density from a finite–width ρ meson [GS form Eq. (A10), $\Gamma_\rho = 0.15\,\text{GeV}$] with $g_{\rho NN} = 3.25$ from the Bonn–Jülich model [37]. Dotted line: Charge density from a zero–width ρ meson pole with the same coupling.

form provides a very good approximation to the charge density over a wide range of b, with an accuracy better than 10% in the range 0.1-1.4 fm. At larger values of b the finite–width density becomes systematically larger than the zero–width approximation, reflecting the fact that large distances are dominated by the spectral strength at the lowest available masses.

The ρ meson contribution to the isovector spectral function in the GS approximation is then given by

$$
\frac{\text{Im}\, F_1^V(t+i0)_\rho}{\pi} = \frac{g_{\rho NN}}{f_\rho}\frac{\text{Im}\, F_{\text{GS}}(t+i0)}{\pi},
\tag{A10}
$$

where $g_{\rho NN}$ is the ρ–meson–nucleon vector coupling, and f_ρ^{-1} parameterizes the ρ meson coupling to the electromagnetic current and is related to the e^+e^- partial decay width as $\Gamma(\rho \to e^+e^-) = (\alpha_{\text{em}} m_\rho/3)(e/f_V)^2$. With the value of $g_{\rho NN} = 3.25$ from the Bonn–Jülich model of the NN interaction [37] and $f_\rho = 5.01$ from the experimental value of the e^+e^- partial decay width [38] we obtain

$$
g_{\rho NN}/f_\rho = 0.65.
\tag{A11}
$$

This value is 30% larger than the simple "vector dominance" value of 0.5, which would follow from normalizing the ρ contribution to the form factor given by Eq. (A10) to $F_1^V(0)_\rho = 1/2$, and reflects the fact that in reality part of the charge carried by the ρ is compensated by the negative contribution from higher–mass states. The spectral function resulting from a ρ meson with this coupling and

a width $\Gamma_\rho = 0.15\,\mathrm{GeV}$ is shown in Fig. 10. One sees that this simple model agrees well with the empirical spectral function in the ρ meson mass region.

Altogether, we see that the chiral component near threshold and the finite–width ρ meson with the above parameters reproduce approximately the empirical isovector spectral function in the different regions. We emphasize that our aim here is not to construct a model of the complete spectral function, but merely to show that the theoretical approximations used in our earlier analysis [8] agree reasonably well with the empirical result *in their respective regions of validity.* In particular, we do not advocate to add the "chiral" and "ρ" components in Fig. 10 (not even with an adjusted ρ meson coupling), as this would imply that one has to evaluate the chiral expression in a region where it is not theoretically justified and compensate the result by subtracting strength elsewhere; cf. the discussion in Ref. [23].

In Fig. 12 we compare the chiral component of the isovector charge density obtained from Eq. (A1) with that generated by the GS finite–width ρ meson with the coupling Eq. (A11). It is seen that the chiral component dominates only at distances $b > 2\,\mathrm{fm}$. An increase of the chiral component by $\sim 20\%$ due to two–loop corrections [23] would not substantially affect this comparison on a logarithmic scale. Also shown in Fig. 12 is the density resulting from a zero–width ρ meson pole of the same coupling, as used in the estimate of Ref. [8]. One notes that the finite width of the ρ meson pushes the region of dominance of the chiral component out to even slightly larger distances. Overall, the refined analysis here fully supports the conclusions of Ref. [8], that the chiral component of the transverse charge density overwhelms the non–chiral density only at distances $b > 2\,\mathrm{fm}$.

[1] For an overview of the early literature, see: J. Bernstein, in: Elementary Particles and Their Currents. Freeman, San Francisco, 1968.

[2] G. A. Miller, Phys. Rev. Lett. **99**, 112001 (2007).

[3] For a review, see: G. A. Miller, Ann. Rev. Nucl. Part. Sci. **60**, 1 (2010).

[4] J. Friedrich and T. Walcher, Eur. Phys. J. A **17**, 607 (2003).

[5] H. W. Hammer, D. Drechsel and U. G. Meissner, Phys. Lett. B **586**, 291 (2004).

[6] C. Crawford *et al.* Phys. Rev. **C82**, 045211 (2010).

[7] D. E. Soper, Phys. Rev. D **15**, 1141 (1977).

[8] M. Strikman and C. Weiss, Phys. Rev. C **82**, 042201 (2010).

[9] S. Venkat, J. Arrington, G. A. Miller, X. Zhan, Phys. Rev. **C83**, 015203 (2011).

[10] M. Burkardt, Phys. Rev. D **62**, 071503 (2000) [Erratum-ibid. D **66**, 119903 (2002)]; Int. J. Mod. Phys. A **18**, 173 (2003).

[11] M. Diehl, Eur. Phys. J. C **25**, 223 (2002) [Erratum-ibid. C **31**, 277 (2003)].

[12] L. Frankfurt, M. Strikman and C. Weiss, Ann. Rev. Nucl. Part. Sci. **55**, 403 (2005).

[13] M. A. Belushkin, H. W. Hammer and U. G. Meissner, Phys. Rev. C **75**, 035202 (2007).

[14] C. F. Perdrisat, V. Punjabi and M. Vanderhaeghen, Prog. Part. Nucl. Phys. **59**, 694 (2007).

[15] G. D. Cates, C. W. de Jager, S. Riordan, B. Wojt-sekhowski, [arXiv:1103.1808 [nucl-ex]].

[16] G. Höhler *et al.*, Nucl. Phys. **B114**, 505 (1976).

[17] M. A. Shifman, A. I. Vainshtein and V. I. Zakharov, Nucl. Phys. B **147**, 385 (1979); **147**, 448 (1979).

[18] G. A. Miller, M. Strikman, C. Weiss, Phys. Rev. **D83**, 013006 (2011).

[19] J. J. Kelly, Phys. Rev. **C70**, 068202 (2004).

[20] G. Hohler, *Pion-nucleon scattering,* in Landolt-Börnstein I/9b2, edited by H. Schopper (Springer, Berlin, 1983).

[21] M. A. Belushkin, H. W. Hammer and U. G. Meissner, Phys. Lett. B **633**, 507 (2006).

[22] J. Gasser, M. E. Sainio, A. Svarc, Nucl. Phys. **B307**, 779 (1988).

[23] N. Kaiser, Phys. Rev. C **68**, 025202 (2003).

[24] C. Bruch, A. Khodjamirian and J. H. Kuhn, Eur. Phys. J. C **39**, 41 (2005).

[25] V. Bernard, N. Kaiser, U. -G. Meissner, Nucl. Phys. **A611**, 429-441 (1996).

[26] G. Hohler and E. Pietarinen, Nucl. Phys. B **95**, 210 (1975).

[27] H. W. Hammer and M. J. Ramsey-Musolf, Phys. Rev. C **60**, 045204 (1999) [Erratum-ibid. C **62**, 049902 (2000)]; **60**, 045205 (1999) [Erratum-ibid. C **62**, 049903 (2000)].

[28] U. G. Meissner, V. Mull, J. Speth and J. W. van Orden, Phys. Lett. B **408**, 381 (1997).

[29] M. Diehl, T. Feldmann, P. Kroll, Phys. Rev. **D77**, 033006 (2008).

[30] M. Vanderhaeghen and T. Walcher, arXiv:1008.4225 [hep-ph].

[31] E. Geis *et al.* [BLAST Collaboration], Phys. Rev. Lett. **101**, 042501 (2008).

[32] S. Riordan *et al.*, Phys. Rev. Lett. **105**, 262302 (2010).

[33] N. Isgur, Phys. Rev. **D59**, 034013 (1999).

[34] G. A. Miller, J. Arrington, Phys. Rev. **C78**, 032201 (2008).

[35] Conceptual Design Report for the Science and Experimental Equipment for the 12 GeV Upgrade of CEBAF, Eds. J. Arrington *et al.*, Jefferson Lab (2005); available at: `http://www.jlab.org/div_dept/physics_division/GeV/doe_review/CDR_for_Science_Review.pdf`

[36] G. J. Gounaris and J. J. Sakurai, Phys. Rev. Lett. **21**, 244 (1968).

[37] R. Machleidt, K. Holinde and C. Elster, Phys. Rept. **149**, 1 (1987).

[38] K. Nakamura et al. (Particle Data Group), J. Phys. G 37, 075021 (2010).

[39] It is possible that some rational form factor fits may give accurate numerical representations of the transverse density up to rather large values of b when used in the Fourier integral Eqs. (2) and (3). However, the range of b for which a given parametrization works depends on the exact location of the singularities in the complex plane, which is determined by the values of the fit parameters and may vary drastically between different fits. One therefore cannot advocate this approach as a general method for studying the densities at large b.

[40] In Ref. [8] we considered the difference of proton and neutron form factors without a factor 1/2. In the present article we follow the standard convention for the isovector and isoscalar form factors with the factor 1/2.

[41] In the fit of Ref. [13] the calculated $\rho\pi$ continuum is approximated by a pole with a mass of 1.125 GeV, practically identical to the pole representing the calculated $K\bar{K}$ continuum and the explicit ϕ contribution, such that all these contributions effectively amount to a single pole at the ϕ mass.

[42] At $b < 0.2$ fm the densities shown in Fig. 9 (dotted line) were calculated as the Fourier integral of the spacelike form factor parametrization of Ref. [13], in order to include the contribution of the highest–mass pole of the form Eq. (11).